

NANOSECOND VELOCITY AND SPATIAL MAP IMAGING USING THE PIXEL IMAGING MASS SPECTROMETRY (PImMS) CAMERA

Michael Burt¹, Jason Lee¹, Kasra Amini¹, Edward Halford¹, Hansjochen Köckert¹, Benjamin Winter¹, Claire Vallance¹, Mark Brouard^{1*}, Steve Thompson², Vic Parr², Rebecca Boll³, Daniel Rolles⁴, and Tatiana Marchenko⁵

¹Department of Chemistry, University of Oxford, Oxford, United Kingdom; ²SAI Ltd., Manchester, United Kingdom; ³Deutsches Elektronen-Synchrotron, Hamburg, Germany; ⁴Department of Physics, Kansas State University, Manhattan, KS, United States of America; ⁵Sorbonne Universités, UPMC Université Paris 06, Paris, France *mark.brouard@chem.ox.ac.uk



UNIVERSITY OF
OXFORD

OVERVIEW

Ion imaging applications of the Pixel Imaging Mass Spectrometry sensor are demonstrated using velocity map imaging and microscope imaging mass spectrometry.

BACKGROUND

Velocity map imaging (VMI) is widely used to investigate the dynamics of small molecules. In these experiments, ions generated with the same kinetic energy are focused onto the same point of a position-sensitive detector.¹ With voltage adjustments, VMI optics can also be used to focus ions with the same initial position, creating an ion microscope.²⁻⁵ Combining these methods with time-of-flight mass spectrometry further allows ions to be separated by their m/z . For VMI, this enables the dynamics of complex molecules to be studied, while the ion microscope can be used for rapid mass spectrometry imaging (MSI).

These techniques have until recently been limited by conventional imaging cameras, which image one m/z per experimental cycle. The development of event-triggered sensors, such as the Pixel Imaging Mass Spectrometry (PImMS) camera, overcome this restriction by enabling every resolved ion to be imaged within one experimental cycle.⁶⁻⁸ Here we report two ion imaging applications of the PImMS sensor: Section I describes microscope MSI, and Section II investigates the photodissociation dynamics of CH_2BrI using VMI.

METHODS

- PImMS is a monolithic sensor that records the (x,y,t) coordinates of incident photons to a precision of 12.5 ns over 50 μs .

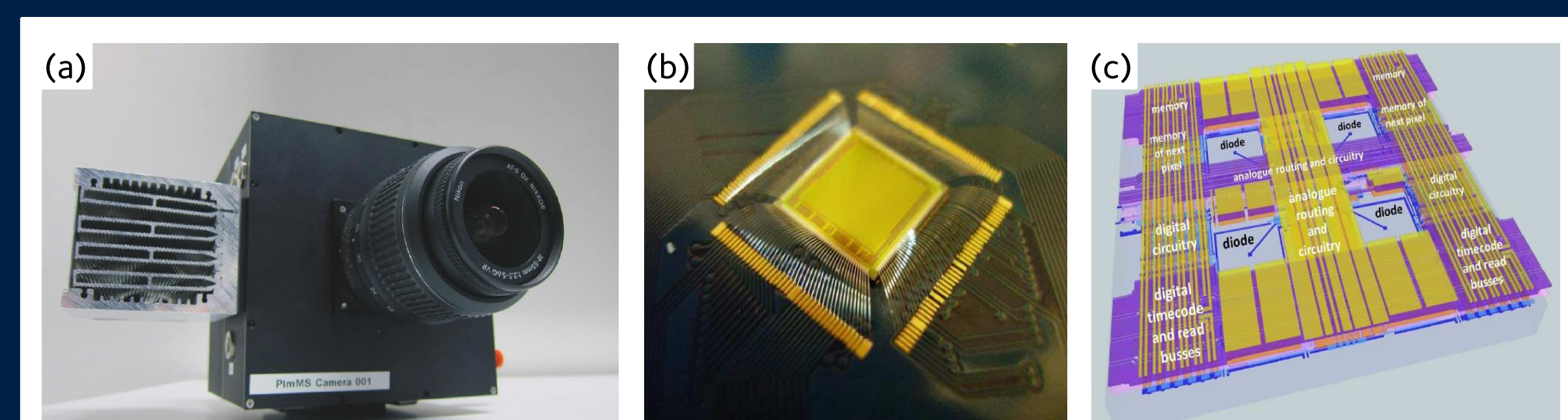


Figure 1: The PImMS camera (a), sensor (b), and sensor diagram (c).

- PImMS sensors are 72x72 (PImMS1) or 324x324 (PImMS2) pixel grids. Each pixel is $70 \times 70 \mu\text{m}^2$ and comprises four diodes measuring $14.5 \times 14.5 \mu\text{m}^2$ (Figure 1).

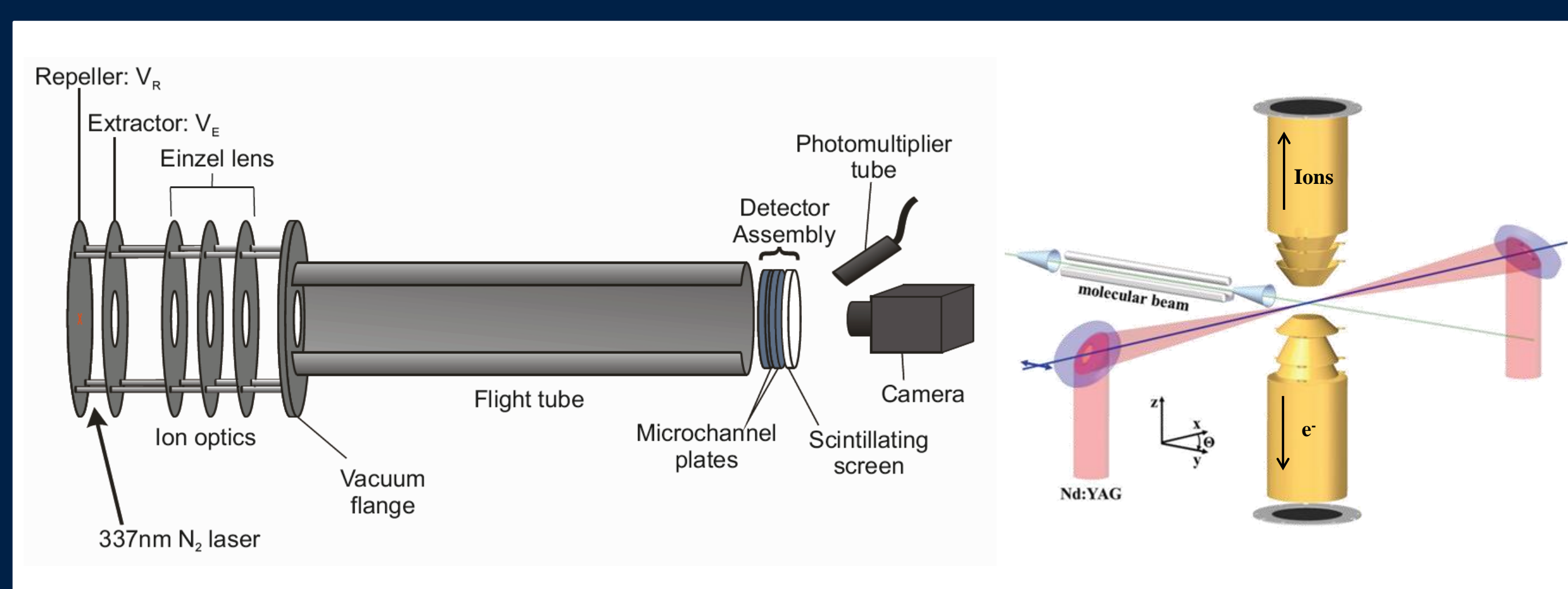


Figure 2: The time-of-flight mass spectrometers used in Sections I (left) and II (right).

- The ion microscope used in Section I is a linear time-of-flight imaging mass spectrometer tuned for spatial imaging. The instrument described in Section II is similar, but is optimized for velocity map imaging. It also has a reflected set of ion optics that allow electrons to be velocity mapped in coincidence with ions (Figure 2).

I. MICROSCOPE IMAGING MS

Microscope imaging uses a defocused laser or ion beam to simultaneously ionize large samples ($1 \times 1 \text{ mm}^2$). Generated ions are then separated by their time-of-flight and electrostatically focused on a two-dimensional detector array, where they are detected as a series of ion images. This complements the multi-mass imaging capability of the PImMS camera, and provides a rapid alternative to conventional microprobe methods (Figure 3).

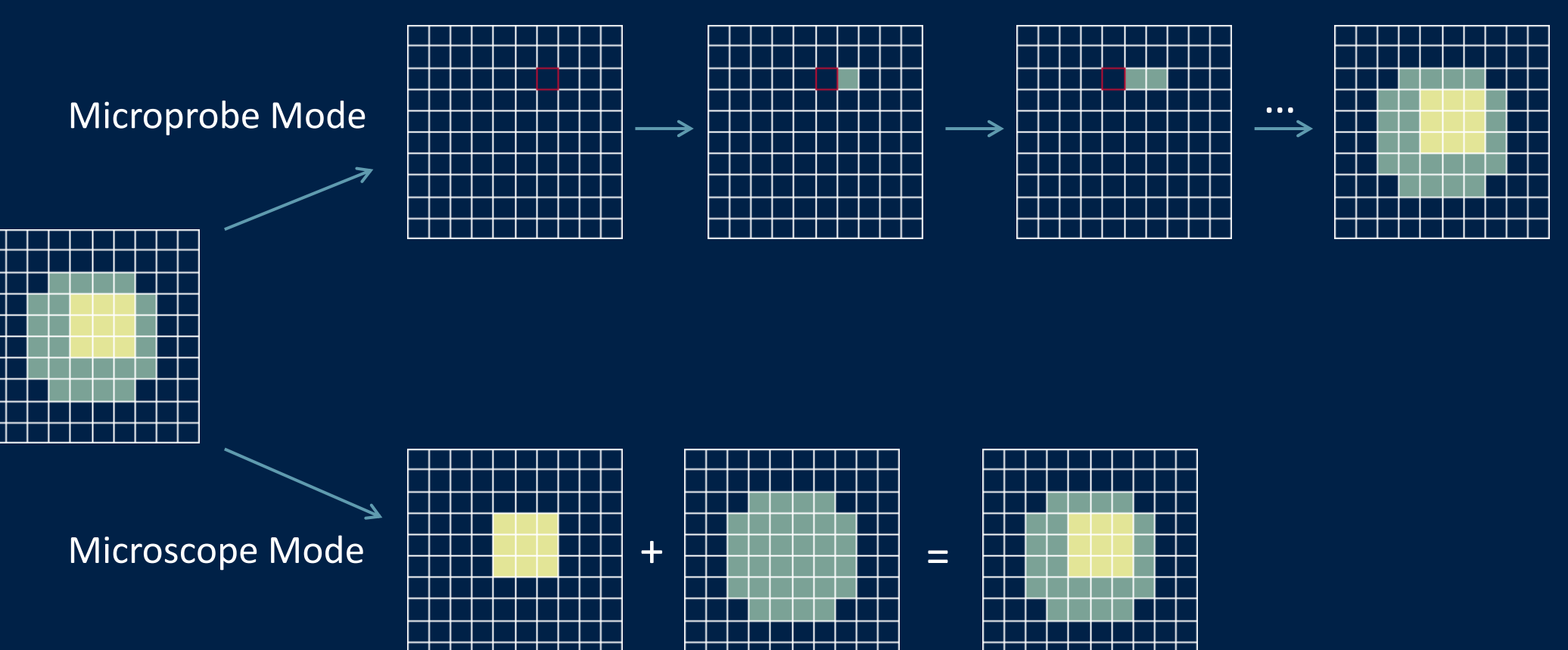


Figure 3: Microprobe and microscope spatial imaging of light (yellow) and heavy (green) molecules on a sample grid. The microscope approach accesses the whole surface simultaneously and is therefore quicker; its resolution is defined by the ion optics, instead of the width of the laser spot (red).

Data were acquired with mass and spatial resolutions of 1 Da and 20 μm for four dyes (Figure 4): (a) Auramine O, (b) Crystal Violet, (c) Exalite 384, and (d) Exalite 404. Surface images of Auramine O and Crystal Violet are shown in Figure 5.⁴

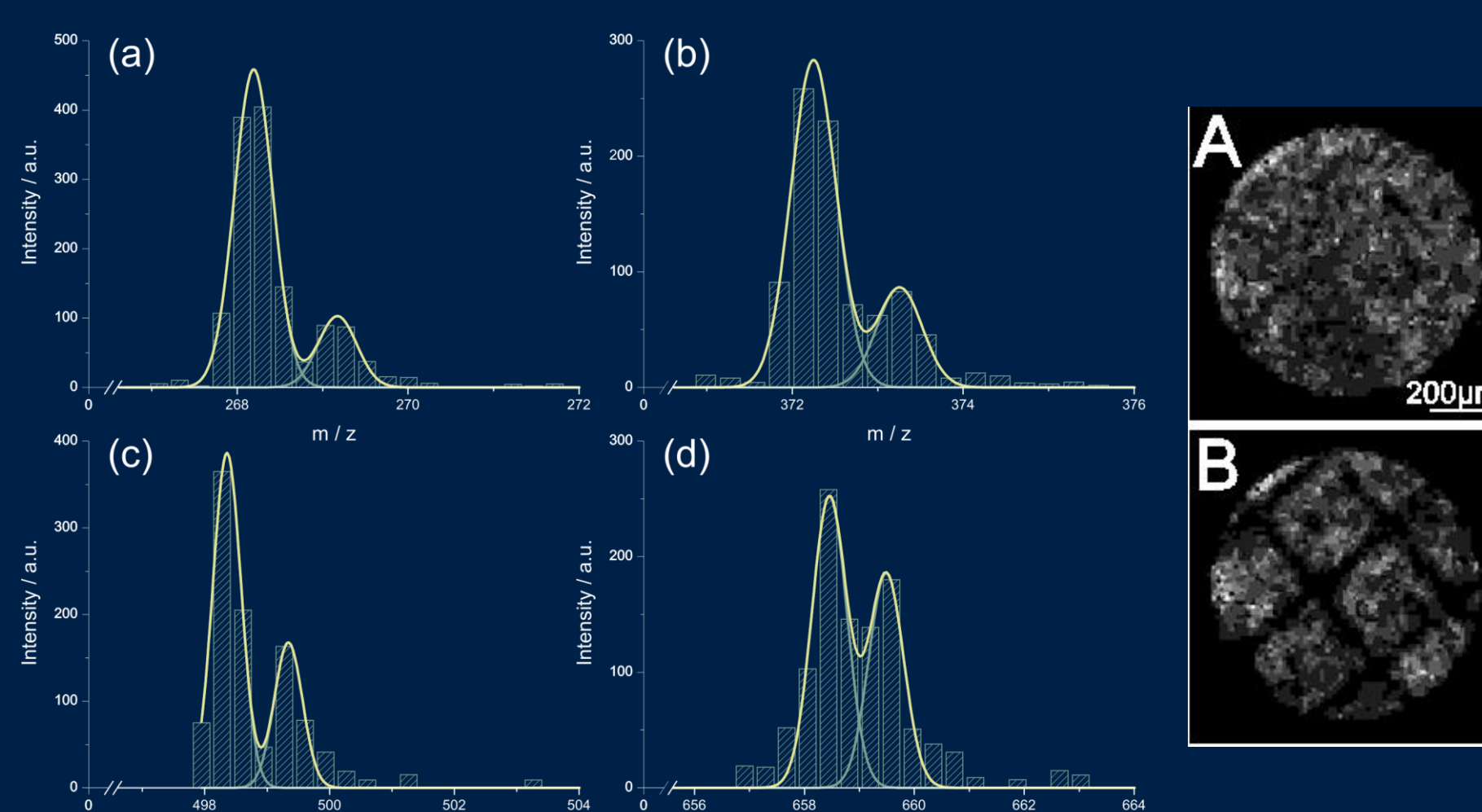


Figure 4 (left): Time-of-flight mass spectra of (a) Auramine O, (b) Crystal Violet, (c) Exalite 384, and (d) Exalite 404. Yellow traces are fits for the time-of-flight peaks.

Figure 5 (right): Spatial images of Auramine O (a) and Crystal Violet (b) acquired during one experiment. The Crystal Violet sample was electrosprayed through a nickel grid.

Microscope imaging may also be applied to more complex species, such as the polyethylene glycol polymer (Figure 6). Comparing this PImMS data with photomultiplier tube (PMT) measurements and the simulated detector response indicates that the resolution of PImMS is below the isotopic limit (Figure 7).

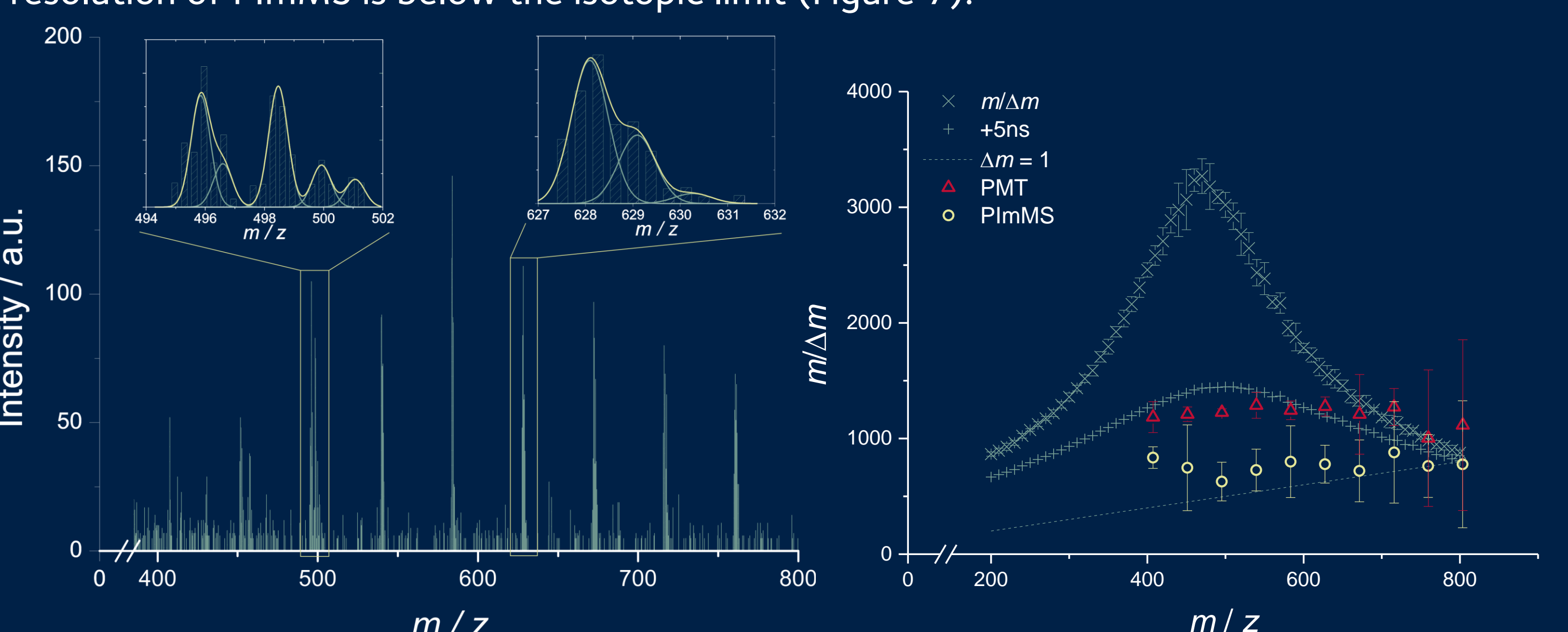


Figure 6 (left): Time-of-flight spectrum of the polyethylene glycol polymer, inset graphs represent two polymers with different sizes. Yellow traces are fits for the time-of-flight peaks.

Figure 7 (right): The resolution of PImMS (yellow) and the PMT (red) are compared to both the isotopic limit ($\Delta m = 1$) and the mass resolution predicted by SIMION 8.0 ($m/\Delta m$). The +5ns trace accounts for the response time of the detector.

II. CH_2BrI PHOTODISSOCIATION DYNAMICS

CH_2BrI photolysis was monitored at the femtosecond scale using a time-dependent $\text{UV}_{266 \text{ nm}} - \text{IR}_{800 \text{ nm}}$ pump-probe scheme. After a set delay following UV absorption, strong field ionization at 800 nm causes the formerly neutral CH_2Br and I fragments to repel.



Coulomb's law dictates that the observed kinetic energy release depends on the distance between the charge centres. Fragment velocities therefore decrease with increasing pump-probe delay, and these were measured using the PImMS camera (Figures 8 and 9).

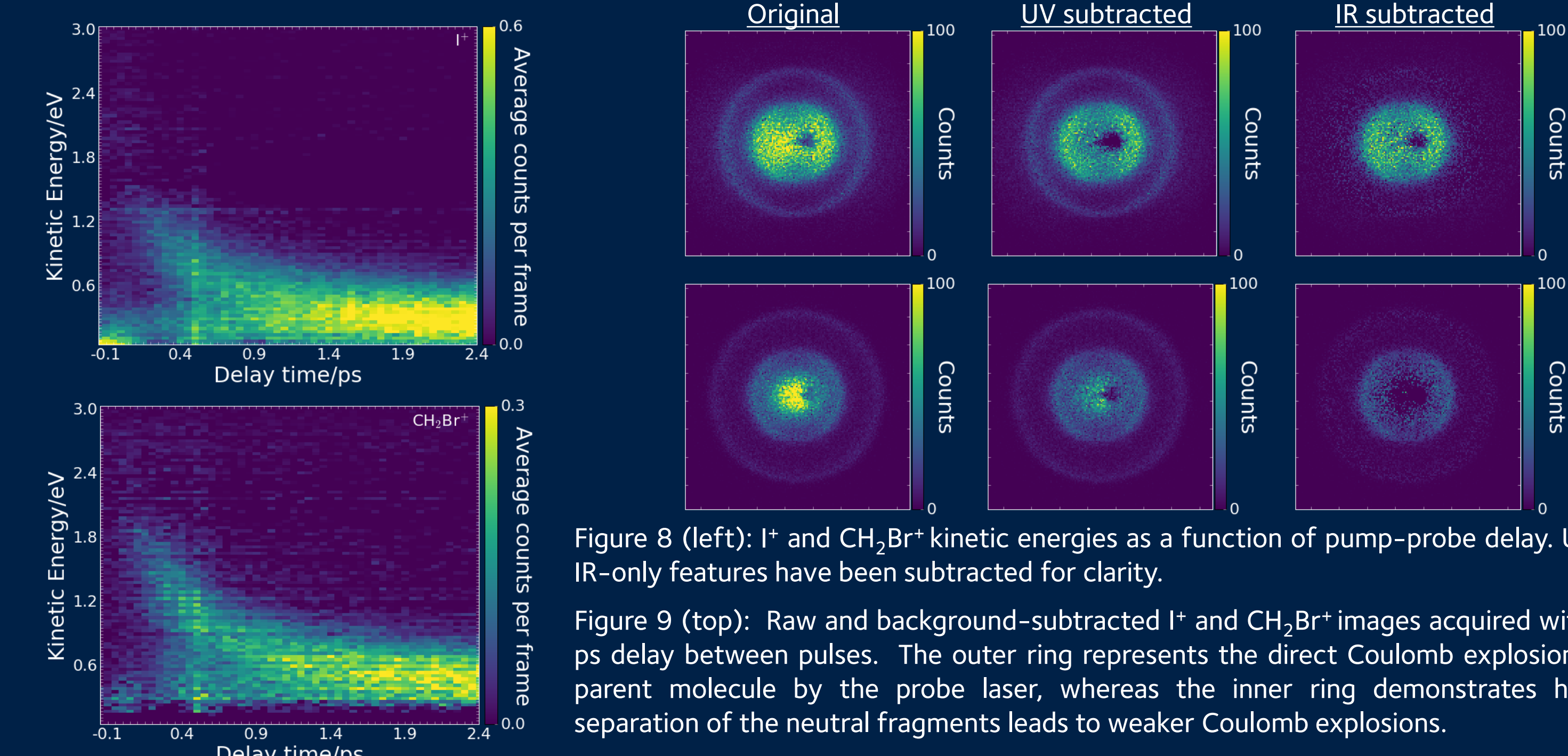


Figure 8 (left): I^+ and CH_2Br^+ kinetic energies as a function of pump-probe delay. UV- and IR-only features have been subtracted for clarity.

Figure 9 (top): Raw and background-subtracted I^+ and CH_2Br^+ images acquired with a 1.8 ps delay between pulses. The outer ring represents the direct Coulomb explosion of the parent molecule by the probe laser, whereas the inner ring demonstrates how the separation of the neutral fragments leads to weaker Coulomb explosions.

The delay-dependent fragment kinetic energy curves can be correlated and used to reconstruct a detailed picture of the CH_2BrI dissociation dynamics (Figures 10 and 11).⁹ The curve shape is sensitive to the charge location on each cofragment, the extent of ionization, the internal excitation of the molecular fragments, and the dissociation lifetime of the molecule.

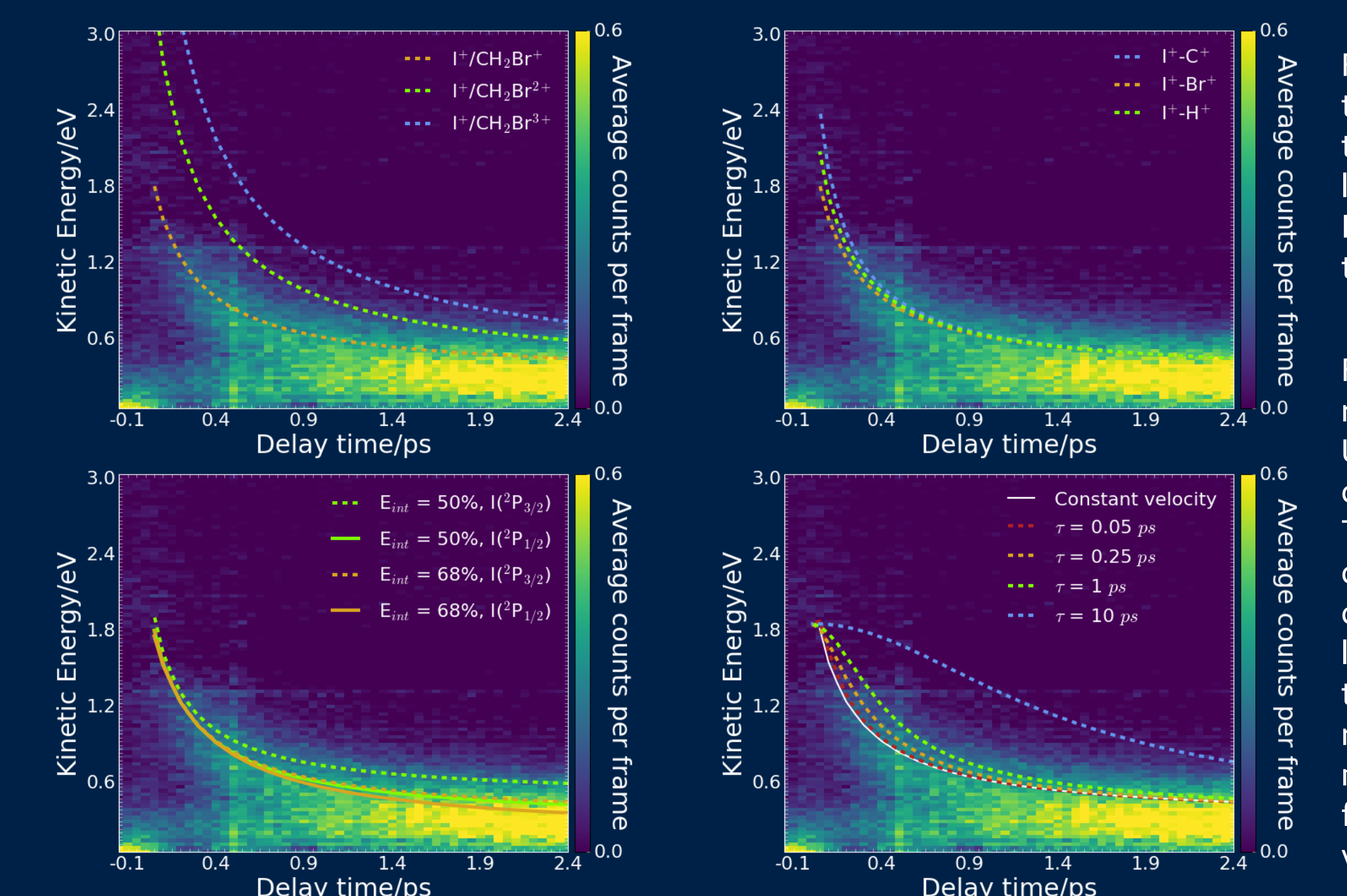
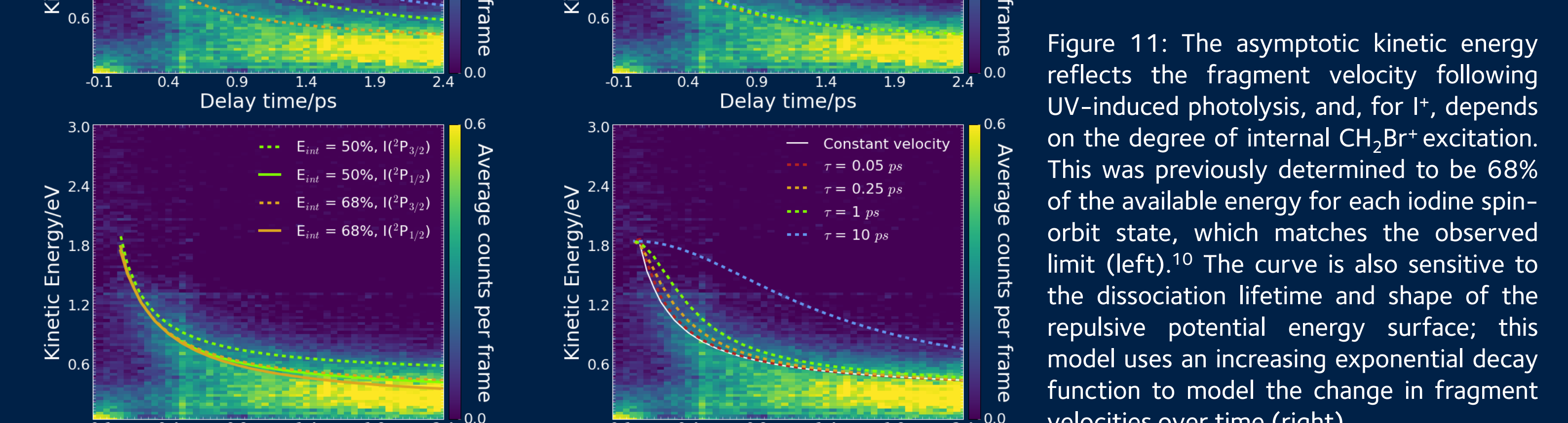


Figure 10: Fragment kinetic energies gained through Coulombic repulsion are sensitive to the cofragment charges (left) and their locations (right). The I^+ curve suggests that I^+ repels against a CH_2Br^+ fragment that has the charge located on Br^+ .



REFERENCES AND ACKNOWLEDGEMENTS

- A. T. J. B. Eppink et al., *Rev. Sci. Instrum.*, 1997, **68**, 3477-3484.
- S. L. Luxemburg et al., *Anal. Chem.*, 2004, **76**, 5339-5344.
- A. Klerk et al., *Int. J. Mass Spectrom.*, 2009, **285**, 19-25.
- E. Halford et al., *Rapid Commun. Mass Spectrom.*, 2014, **28**, 1649-1657.
- B. Winter et al., *Int. J. Mass Spectrom.*, 2013, **356**, 14-23.
- J. J. John et al., *J. Instrum.*, 2012, **7**, C08001.
- T. Clark et al., *J. Phys. Chem. A*, 2012, **116**, 10897-10903.
- This work is subject to a patent application by ISIS Innovations Ltd.; patent publication number US20100294924A1.
- B. Erk et al., *Science*, 2014, **345**, 288-291.
- L. Butler et al., *J. Chem. Phys.*, 1987, **86**, 2051-2074.